Excited-state quantum phase transitions and Loschmidt-echo spectra in a spinor Bose-Einstein condensate

Zhen-Xia Niu[1] and Qian Wang[1,2,*]

[1]*Department of Physics, Zhejiang Normal University, Jinhua 321004, China*

[2]*CAMTP-Center for Applied Mathematics and Theoretical Physics, University of Maribor, Mladinska 3, SI-2000 Maribor, Slovenia*

(Received 28 November 2022; accepted 23 February 2023; published 8 March 2023)

Identifying dynamical signatures of excited-state quantum phase transitions (ESQPTs) in experimentally realizable quantum many-body systems is helpful for understanding the dynamical effects of ESQPTs. In such systems, the highly controllable spinor Bose-Einstein condensates (BECs) offer an exceptional platform to study ESQPTs. In this work, we investigate the dynamical characteristics of the ESQPT in spin-1 BEC by means of the Loschmidt echo spectrum. The Loschmidt echo spectrum is an extension of the well-known Loschmidt echo and defined as the overlaps between the evolved state and the excited states of the initial Hamiltonian. We show that both the time-evolved and long-time-averaged Loschmidt echo spectrum undergo a remarkable change as the system passes through the critical point of the ESQPT. Moreover, the particular behavior exhibited by the Loschmidt echo spectrum at the critical point stands as a dynamical detector for probing the ESQPT. We further demonstrate how to capture the features of the ESQPT by using the energy distribution associated with the Loschmidt echo spectrum for time-evolved and long-time-averaged cases, respectively. Our findings contribute to a further verification of the usefulness of the Loschmidt echo spectrum for witnessing various quantum phase transitions in many-body systems and provide a different way to experimentally examine the dynamical consequences of ESQPTs.

DOI: 10.1103/PhysRevA.107.033307

I. INTRODUCTION

Understanding the notion of excited-state quantum phase transitions (ESQPTs) in quantum many-body systems has attracted a lot of interest in recent years [1–6]. As a generalization of the ground-state quantum phase transition (QPT) [7] to excited states, ESQPTs exist in a wide range of quantum many-body systems, including the interacting boson model [2,8–10], molecular bending transitions [11–13], the kicked and coupled top models [14–17], the Kerr-nonlinear oscillator [18,19], the spinor Bose-Einstein condensates (BECs) [20–24], the Lipkin-Meshkov-Glick (LMG) model [2,25–30], as well as the Dicke and Rabi models [31–35].

ESQPTs are characterized by singularities in the density of states (DOS). The energy that leads to the divergence of the DOS is identified as the ESQPT critical energy. In contrast to the standard QPT, which describes an unsmooth variation of a system's ground-state properties with a control parameter, an ESQPT shows strong effects on a large amount of excited states and results in nonanalytical evolution in their structure and energy with both the energy and control parameter. Although ESQPTs extend the QPTs to excited states, they can take place in the systems with no QPT [36–38]. The ESQPT occurs only in the thermodynamic limit, but its emergence can be revealed by scaling analyses in finite systems. It is worth pointing out that various studies on ESQPTs are focused on the systems that are associated with classical counterparts having a few degrees of freedom, however, the definition of ESQPTs for any number of degrees of freedom was investigated by the authors of Ref. [4].

The close connection between ESQPTs and several fundamental questions in diverse areas of modern physics has led the study of ESQPTs to become a quite active research field. There is a vast amount of theoretical studies on the effects of ESQPTs. It was known that ESQPTs can strongly affect the quantum dynamics after a quench [31,37,39–45], localize the eigenstates [29,30], accelerate the time evolution of the system [46–48], and create the Schrödinger cat states [38]. ESQPTs are also closely related to the onset of chaos [15,49–51] and different types of dynamical quantum phase transitions [52–54], as well as the thermal phase transition [55]. The particular role played by the ESQPTs in the thermalization process of isolated quantum systems has also been revealed recently [56,57]. Moreover, the endeavor to explore the order parameters of ESQPTs [6,21,33,42,58] provides further insights into the excited-state phases.

To date, ESQPTs were experimentally observed in molecular bending transitions [11,12] and microwave Dirac billiards [59] via the singularities in the DOS. However, none of these systems allows us to experimentally probe the dynamical signatures of ESQPTs in a controllable way. In this context, spinor BECs [60,61] provide excellent platforms to study the dynamical signatures of ESQPTs, because they have a high degree of controllability [62–67] and show ESQPTs in their spectra [20–22,24]. While signatures of the ground-state QPT and associated dynamical features in spinor BECs were

*qwang@zjnu.edu.cn

theoretically analyzed [60,61,68–71] and observed in numerous experiments [67,72–78], only a few recent studies were concerned with the characteristics of ESQPTs [21–23].

In this work, we investigate the dynamical signatures of ESQPT in the spin-1 BEC using the Loschmidt echo spectrum, which was proposed in a very recent work [79]. The Loschmidt echo spectrum extends the conventional concept of the Loschmidt echo beyond the ground state and is defined as the overlaps between the evolved state and the excited states. As the dynamics in a quantum system is governed by its entire energy spectrum, one can expect that the Loschmidt echo spectrum will offer more dynamical characteristics of the system. Since the ESQPT typically affects the full spectrum of excited states, it is expected that more insights into the dynamical properties of ESQPT can be obtained through the Loschmidt echo spectrum. The usefulness of the Loschmidt echo spectrum in studying of the dynamical quantum phase transitions (DQPTs) in spin systems has been verified [79], which shows that the Loschmidt echo spectrum not only behaves as a powerful detector of DQPTs but also helps us to get a better understanding on the physical nature of DQPTs. Here, we examine its ability to characterize the ESQPT. To the best of our knowledge, the Loschmidt echo spectrum has not been used to explore the dynamical signatures of the ESQPT in previous works.

The ESQPT in the spin-1 BEC is signified by the logarithmic divergence of the DOS and it can lead to an abrupt change in the structure of eigenstates. The analysis of the classical limit of the system shows that the onset of ESQPT can be considered as a consequence of the saddle point in its classical counterpart. We show that the underlying ESQPT exhibits strong impact on the time evolution of the Loschmidt echo spectrum. Both the existence and different phases of the ESQPT can be reliably identified by the properties of the Loschmidt echo spectrum and associated energy distribution. We further display how the ESQPT manifests itself in the long-time-averaged Loschmidt echo spectrum and associated energy distribution. The aim of the present work is to access the signatures of ESQPT from both time-evolved and long-time-averaged behaviors of the Loschmidt echo spectrum, as well as to provide further evidence of the validity of the Loschmidt echo spectrum for diagnosing various phase transitions in quantum many-body systems.

The rest of the article is structured as follows. In Sec. II, we introduce the considered physical system and its classical limit and discuss the basic features of the ESQPT. Our main results are presented in Sec. III, where we report the properties of the Loschmidt echo spectrum and associated energy distribution, and reveal their connection with the ESQPT for time-evolved and long-time-averaged cases, respectively. Finally, we summarize our results and conclude in Sec. IV.

II. QUANTUM SYSTEM

We consider the spin-1 BEC, which describes N mutually interacting atoms with three hyperfine spin states $m = 0, \pm 1$ and can be experimentally realized by ^{87}Rb and ^{23}Na atoms [60,61]. Using the single-mode approximation [60] which decouples the spin and spatial degrees of freedom, the Hamiltonian of the system can be written as [60,61]

$$\frac{\hat{H}}{|c|} = \frac{\mathrm{sign}(c)}{N}\Big[\hat{a}_0^{\dagger 2}\hat{a}_1\hat{a}_{-1} + \hat{a}_1^{\dagger}\hat{a}_{-1}^{\dagger}\hat{a}_0^2 + \hat{N}_0(\hat{N}_1 + \hat{N}_{-1}) + \frac{1}{2}(\hat{N}_1 - \hat{N}_{-1})^2\Big] + \kappa(\hat{N}_1 + \hat{N}_{-1}). \quad (1)$$

Here, $\hat{a}_m(\hat{a}_m^{\dagger})$ with $m = 0, \pm 1$ are the bosonic annihilation (creation) operators for spin state m, $\hat{N}_m = \hat{a}_m^{\dagger}\hat{a}_m$ denote the atom number operators and satisfy $\sum_m \hat{N}_m = \hat{N}$. The parameter c refers to the strength of the interspin interaction with $c < 0$ ($c > 0$) for ferromagnetic (antiferromagnetic) BEC [60], while $\kappa \equiv q/|c|$ represents the effective quadratic Zeeman shift and can take both positive and negative values by means of microwave dressing [64,66].

The Hamiltonian (1) conserves the magnetization $\hat{\mathcal{M}}_z = \hat{N}_1 - \hat{N}_{-1}$ and parity $(-1)^{\hat{N}_0}$ [21]. In this work, we restrict our analysis to the even parity subspace with $\mathcal{M}_z = 0$, thus the Hilbert space has dimension $\mathcal{D}_{\mathcal{H}} = N/2 + 1$. Moreover, we only consider the ferromagnetic spinor BEC with $c < 0$ and $\kappa \geqslant 0$. However, we would like to point out that it is straightforward to generalize our studies to the cases of antiferromagnetic spinor condensate, $\mathcal{M}_z \neq 0$ and $\kappa < 0$.

For our considered case, it is known that the system exhibits a ground-state QPT at the critical point $\kappa_c = 2$, which divides the broken-axisymmetry phase with $\kappa < 2$ from the polar phase with $\kappa > 2$ [61,69–73]. In addition, the existence of ESQPTs and the relevant signatures and applications in spinor BECs were also investigated in recent works [20–22,24].

The main characteristics of ESQPT in spin-1 BEC have been unveiled [21]. In the following subsections, we will briefly review the results in Ref. [21] and perform further analysis on the features of the ESQPT by focusing on the eigenstates' localization property in both the quantum and classical cases.

A. Excited-state quantum phase transitions

ESQPTs are signified by the clustering of the eigenlevels, which results in the singularities in the DOS [2,5]. To illustrate the ESQPT in the spin-1 BEC, we analyze the spectrum of Hamiltonian (1) as a function of control parameter κ. In Fig. 1(a), we show how the rescaled excitation energies, $\varepsilon_n = (E_n - E_0)/N$, evolve with increasing κ. Here, E_n denotes the nth eigenenergy of $\hat{H}$ and E_0 is its ground-state energy. One can see that the excited eigenlevels exhibit an obvious cluster along the dot-dashed line, which marks the critical energy of the ESQPT, denoted by ε_c. We further observe that the critical energy ε_c decreases with increasing κ and moves towards to the known ground-state QPT as κ approaches 2. By utilizing the mean-field approximation, the explicit dependence of the critical energy ε_c on the control parameter κ can be obtained analytically [see Eq. (5) below]. As a consequence of the eigenlevels' cluster, the DOS, $\rho(\varepsilon) = \sum_n \delta(\varepsilon - \varepsilon_n)$, shows a sharp peak at ε_c for the cases of $\kappa < 2$, as visualized in Figs. 1(b) and 1(c). In the $N \to \infty$ limit, the peak in the DOS turns into a logarithmic divergence, which makes up a prominent signature of the ESQPT.

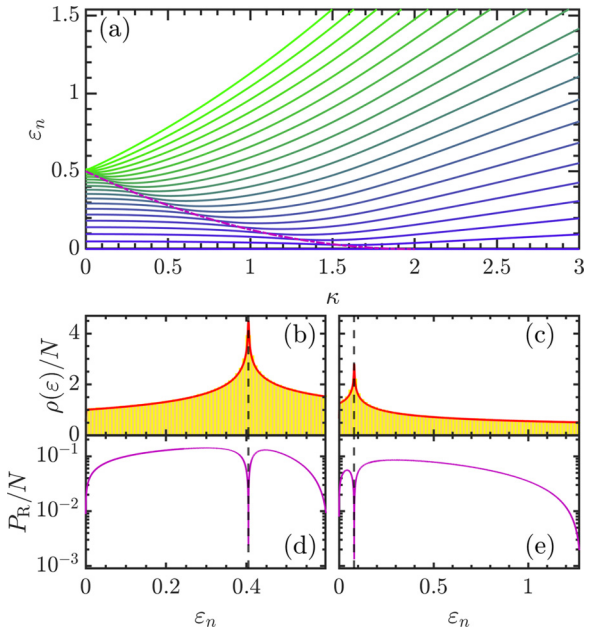

FIG. 1. (a) Rescaled energy levels $\varepsilon_n = (E_n - E_0)/N$ as a function of κ with $N = 40$. The purple dot-dashed line denotes the critical energy of ESQPT, as given in Eq. (5). (b), (c) Normalized density of states $\rho(\varepsilon)/N$ for (b) $\kappa = 0.2$ and (c) $\kappa = 1.2$ with $N = 10\,000$. The red solid lines are the analytical results, see Eq. (6). (d), (e) Rescaled participation ratio P_R/N as a function of ε_n for the same values of κ as in panels (b), (c) with $N = 10\,000$. The vertical dashed lines in panels (b)–(e) represent the critical energy of the ESQPT obtained from Eq. (5).

The emergence of the ESQPT is also closely connected with the localization of the eigenstates, namely, the eigenstates in the neighborhood of ε_c are the highly localized states [29,30]. The degree of localization of the eigenstates $|\psi_n\rangle$ for a given basis $\{|\alpha_k\rangle\}$ is measured by the participation ratio $P_R = 1/\sum_k |c_k^{(n)}|^4$, where $c_k^{(n)} = \langle\alpha_k|\psi_n\rangle$. For the spin-1 BEC, the basis consists of the Fock states $|\alpha_k\rangle = |N_{-1}, N_0, N_1\rangle$. The extended state has a larger value of P_R, while a small P_R indicates the localized state. Figures 1(d) and 1(e) plot the rescaled participation ratio as a function of ε_n for different control parameters. A sharp dip in the behavior of P_R at $\varepsilon_n \sim \varepsilon_c$ is clearly visible. The appearance of dip in P_R means that the eigenstate at the critical energy is localized in the Fock basis.

B. Classical limit

More insights into the characteristics of the ESQPT can be obtained by analyzing the properties of the stationary points in the corresponding classical system. To derive the classical counterpart of the Hamiltonian (1), we first note that in the classical limit with $N \to \infty$, the spin states are described by the coherent states [21,24,80]

$$|\boldsymbol{\xi}\rangle = \frac{1}{\sqrt{N!}}(\xi_{-1}a_{-1}^\dagger + \xi_0 a_0^\dagger + \xi_1 a_1^\dagger)^N|0\rangle, \tag{2}$$

where $|0\rangle$ is the vacuum state, $\xi_m = \sqrt{N_m}e^{i\varphi_m}$ with $\varphi_m \in [-\pi, \pi)$ and $\sum_m N_m = N$. Then by using the relation $\langle\boldsymbol{\xi}|a_m|\boldsymbol{\xi}\rangle = \xi_m$, it is straightforward to find that the classical

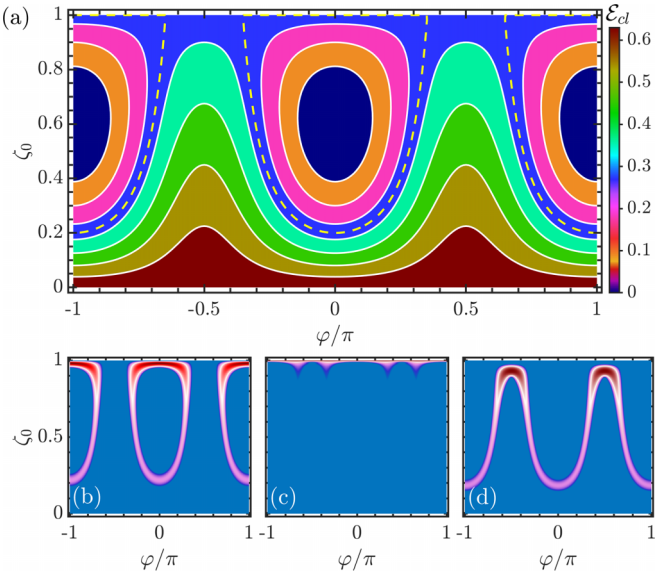

FIG. 2. (a) Energy contours of the classical Hamiltonian (3) in the phase space. The yellow dashed line denotes the separatrix given by Eq. (5). (b)–(d) Rescaled Husimi distributions, $\mathcal{Q}(\zeta_0, \varphi) = Q(\zeta_0, \varphi)/Q_{\max}(\zeta_0, \varphi)$ for (b) $\varepsilon_n = 0.2909$, (c) $\varepsilon_n = \varepsilon_c = 0.32$, and (d) $\varepsilon_n = 0.347$ with $N = 300$. Other parameter: $\kappa = 0.4$.

Hamiltonian with $N_{-1} = N_1$ is given by [21,60,81]

$$H_{cl} = \lim_{N\to\infty} \frac{\langle\boldsymbol{\xi}|\hat{H}|\boldsymbol{\xi}\rangle}{N} = \kappa(1-\zeta_0) - 2\zeta_0(1-\zeta_0)\cos^2\varphi, \tag{3}$$

where $\zeta_0 = N_0/N$ and $\varphi = \varphi_0 - (\varphi_1 + \varphi_{-1})/2$. The classical equations of motion are, therefore, given by

$$\dot{\varphi} = \frac{\partial H_{cl}}{\partial \zeta_0} = -\kappa - 2(1-2\zeta_0)\cos^2\varphi,$$
$$\dot{\zeta}_0 = -\frac{\partial H_{cl}}{\partial \varphi} = -2\zeta_0(1-\zeta_0)\sin(2\varphi), \tag{4}$$

with the constrained condition $d(\varphi_1 - \varphi_{-1})/dt = 0$.

By setting $\dot{\varphi} = \dot{\zeta}_0 = 0$, one can find that the classical system (3) has three fixed points when $\kappa < 2$. They are two stable points $\{\cos\varphi, \zeta_0\} = \{\pm 1, (2+\kappa)/4\}$ with the minimal energy of the classical system $\mathcal{E}_{\min} = -(\kappa-2)^2/8$, and a saddle point at $\zeta_0 = 1$ with energy $\mathcal{E}_s = 0$. In Fig. 2(a), we plot the energy contours in phase space for the classical system. We observe two different structures in the energy surface. The change in the structure of the classical energy surface indicates the presence of the separatrix in the classical dynamics. The equation of the separatrix in Fig. 2(a) is determined by the energy difference $\mathcal{E}_s - \mathcal{E}_{\min}$, which also corresponds to the critical energy of the ESQPT,

$$\varepsilon_c = \frac{(\kappa-2)^2}{8}, \tag{5}$$

with $0 < \kappa < 2$. This result was plotted as the purple dot-dashed line in Fig. 1(a).

The agreement between the separatrix and the critical energy of the ESQPT implies that the logarithmic divergence in the DOS is a consequence of the saddle point in the underlying classical counterpart. To see this, we consider the semiclassical approximation of the DOS in the subspace with

$N_{-1} = N_1$ [21],

$$\frac{\rho_{cl}(\varepsilon)}{N} = \frac{1}{(2\pi)^3}\int \mathcal{D}\boldsymbol{\xi}\delta(\zeta_{-1}-\zeta_1)\delta(\varepsilon - H_{cl}), \tag{6}$$

where $\mathcal{D}\boldsymbol{\xi} = \prod_m d\zeta_m d\varphi_m \delta(\sum_k \zeta_k - 1)$. Here, we would like to point out that $\rho_{cl}(\varepsilon)$ provides the smooth component in the Gutzwiller trace formula [82]. The integral in the above equation can be carried out by employing the property of the delta-function and the final results for different control parameters κ are plotted as the red solid lines in Figs. 1(b) and 1(c). We see an excellent agreement between the numerical data and the behavior of $\rho_{cl}(\varepsilon)/N$. In particular, $\rho_{cl}(\varepsilon)/N$ shows an obvious singularity at the critical energy of the ESQPT.

The existence of the saddle point in the classical system also explains the localization at the critical energy of the ESQPT. To see this, we consider the localization behavior of an eigenstate $|\varepsilon_n\rangle$ in the classical phase space, which can be visualized by the Husimi distribution [83]

$$Q(\zeta_0, \varphi) = |\langle\varepsilon_n|\boldsymbol{\xi}\rangle|^2. \tag{7}$$

It is known that the Husimi distribution $Q(\zeta_0, \varphi)$ offers the quasiprobability distribution of $|\varepsilon_n\rangle$ in the classical phase space with canonical variables (ζ_0, φ).

Figures 2(b) to 2(d) plot the Husimi distribution for the eigenstates with energy below, at, and above the crtical energy of the ESQPT. For the eigenstate with the critical energy of the ESQPT [Fig. 2(c)], the Husimi distribution displays a highly concentrated feature in the phase space. By contrast, the Husimi distribution for the eigenstates with energy below and above the ESQPT is extended in the phase space, as seen in Figs. 2(b) and 2(d), respectively. The behaviors of the Husimi distribution for different eigenstates are consistent with the variation of the participation ratio with the eigenenergy.

III. LOSCHMIDT ECHO SPECTRUM AND ESQPT

In the rest of the article, we analyze the dynamical signatures of the ESQPT by means of the Loschmidt echo spectrum. To this end, we assume that the system is initially prepared in the ground state $\rho(0) = |\psi_0\rangle\langle\psi_0|$ of $\hat{H}_i$ with $\kappa = \kappa_i$. Then, at $t = 0$, we suddenly change the control parameter to a new value $\kappa = \kappa_i + \delta\kappa$ and focus on the dynamics of the system governed by the postquench Hamiltonian $\hat{H}_f$. As the changing of the control parameter κ leads to the varying energy in the system, one can drive the system crossing different phases of the ESQPT by tuning the value of $\delta\kappa$. The critical quench strength, denoted by $\delta\kappa_c$, is defined as the one that takes the system to the critical energy of the ESQPT. Employing the mean-field approximation, one can find $\delta\kappa_c$ is given by

$$\delta\kappa_c = 1 - \frac{\kappa_i}{2}, \tag{8}$$

where $0 \leqslant \kappa_i \leqslant 2$. At this point, it is worth pointing out that our conclusions of this work are independent of the choice of κ_i as long as $0 \leqslant \kappa_i \leqslant 2$. Here, as we are focused only on investigating the dynamical features of ESQPT, the analysis on the cases with $\kappa_i > 2 (< 0)$ are left for future study. We stress that employing the Loschmidt echo spectrum to explore the quantum many-body dynamics for the critical line crossing quenches in the spinor BECs remains an open question. It was experimentally observed that the spin-1 BEC undergoes dynamical phase transitions as the control parameter quenches from the antiferromagntic (AFM) region [20]. Hence, one can expect to find an abrupt change in the behavior of the Loschmidt echo spectrum for quenches that cross the critical line.

After quench, the state of the system at time t is $\rho(t) = e^{-i\hat{H}_f t}\rho(0)e^{i\hat{H}_f t}$. To extract the dynamical signatures of the ESQPT from $\rho(t)$, we use the Loschmidt echo spectrum [79]

$$L_n(t) = \mathrm{Tr}[\rho_n\rho(t)] = \left|\sum_\alpha \langle\psi_n|\alpha\rangle\langle\alpha|\psi_0\rangle e^{-iE_\alpha t}\right|^2, \tag{9}$$

where $\rho_n = |\psi_n\rangle\langle\psi_n|$ is the nth eigenstate of $\hat{H}_i$ with associated energy E_n and $|\alpha\rangle$ is the αth eigenstate of the postquench Hamiltonian $\hat{H}_f$ with the corresponding eigenenergy E_α, so that $\hat{H}_f|\alpha\rangle = E_\alpha|\alpha\rangle$.

The Loschmidt echo spectrum measures how the time-evolved state spreads in the eigenstates of the initial Hamiltonian and its ability to probe the dynamical quantum phase transitions in quantum many-body systems was investigated in a very recent work [79]. Since the ESQPT involves the entire energy spectrum of the system, we would expect that more dynamical signatures of the ESQPT can be revealed by the Loschmidt echo spectrum. Notice that the zero component of the Loschmidt echo spectrum, L_0, is the well-known survival probability, which has been widely used as a dynamical detector of ESQPTs [29–31,37,43–46,84].

Figsures 3(a) to 3(c) demonstrate how the Loschmidt echo spectrum evolves as a function of t for different quench strength $\delta\kappa$ with the system size $N = 1000$ and $\kappa_i = 0.4$, which determines $\delta\kappa_c = 0.8$. For the case with $\delta\kappa < \delta\kappa_c$, as illustrated in Fig. 3(a), the small quench strength can only scatter the quenched state into the low excited states of the initial Hamiltonian. As a consequence, the Loschmidt echo spectrum is highly concentrated in the low H_i eigenenergies, irrespective of the time. Moreover, small $\delta\kappa$ value also leads to the revival of the initial state, which results in the regular oscillations in t of the Loschmidt echo spectrum. With increasing $\delta\kappa$, more excited states are involved and the number of excited states contributing to the Loschmidt echo spectrum increases. Once the critical quench $\delta\kappa_c = 0.8$ is reached, the Loschmidt echo spectrum quickly spreads out over a larger number of excited eigenenergies and shows a complex dependence on the time, as seen in Fig. 3(b). The fast spread of the Loschmidt echo spectrum at the critical quench can be considered as a result of the saddle point in the corresponding classical system, which gives rise to the dynamical instability in the quantum system [47,48,85–88]. As $\delta\kappa$ increases further, such as $\delta\kappa = 1.2$ case shown in Fig. 3(c), the Loschmidt echo also distributes over a wider range of excited eigenenergies, while it initially shows a regular oscillations which is followed by an irregular pattern at later times. The regular behavior in the evolved Loschmidt echo spectrum is a consequence of the periodic trajectories in the underlying classical dynamics, while the long time irregular oscillations are due to the quantum interference effect on the evolution of the Loschmidt echo spectrum.

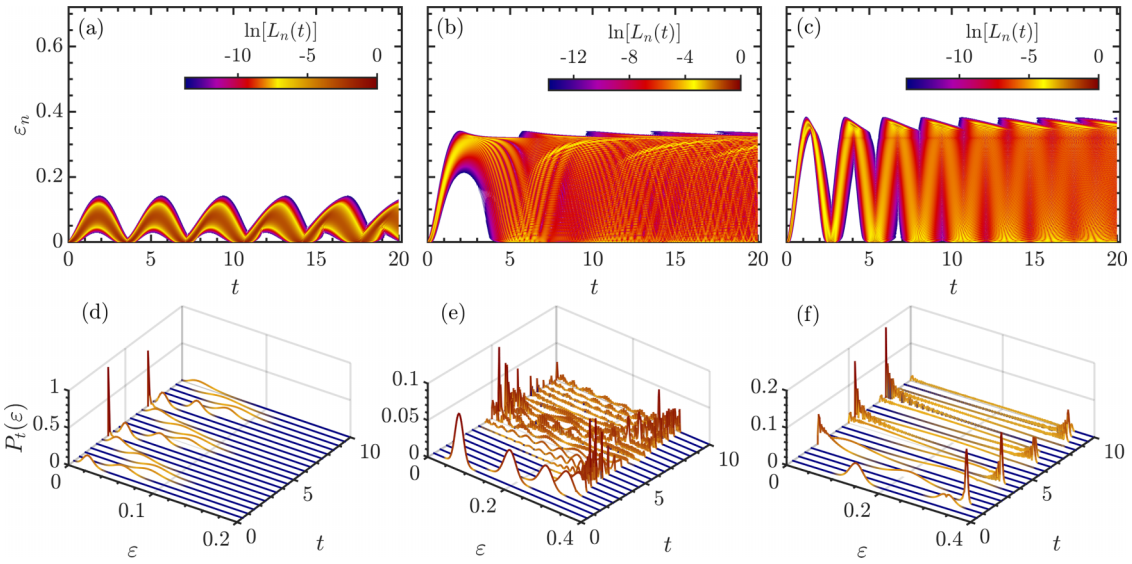

FIG. 3. (a)–(c) Color plot of the Loschmidt echo spectrum (in logarithmic scale) as a function of t and ε_n for (a) $\delta\kappa = 0.4$, (b) $\delta\kappa = \delta\kappa_c = 0.8$, and (c) $\delta\kappa = 1.2$. In each panel, the white regions denote $L_n(t) = 0$. (d)–(f) Evolving of the energy distribution $P_t(\varepsilon)$ [cf. Eq. (10)] as a function of t for the same values of $\delta\kappa$ as in panels (a)–(c). Other parameters: $N = 1000$, $\kappa_i = 0.4$, and $\delta\kappa_c = 0.8$ [see Eq. (8)].

A. Energy distribution of the evolved state

The dynamical features observed in Figs. 3(a) to 3(c) are more visible in Figs. 3(d) to 3(f), where we plot the time evolution of the energy distribution of the evolved state weighted by components $L_n(t)$,

$$P_t(\varepsilon) = \sum_n L_n(t)\delta(\varepsilon - \varepsilon_n). \tag{10}$$

It can be considered as the vertical cutting version of the evolved $L_n(t)$ at a fixed time and satisfies $\int d\varepsilon P_t(\varepsilon)$=1. We see that the evolution of $P_t(\varepsilon)$ shows an obvious difference between two phases of the ESQPT. Hence, different phases of the ESQPT can be distinguished by the distinct behaviors in the evolved $P_t(\varepsilon)$ for $\delta\kappa < \delta\kappa_c$ and $\delta\kappa > \delta\kappa_c$, respectively. In addition, the singular behavior of $P_t(\varepsilon)$ at the critical quench stands as a faithful figure of merit for diagnosing the presence of the ESQPT.

A main feature exhibited by $P_t(\varepsilon)$ is the different degrees of extension over the excited eigenenergies, which can be quantified by the variance of $P_t(\varepsilon)$ with the definition given by

$$\Sigma(t) = \int d\varepsilon P_t(\varepsilon)[\varepsilon - \langle\varepsilon\rangle]^2, \tag{11}$$

where $\langle\varepsilon\rangle = \int d\varepsilon P_t(\varepsilon)\varepsilon$ is the averaging of ε.

Figure 4(a) plots the variance of $\Sigma(t)$ with increasing t for three different quench strengths, which are below, at, and above the critical quench strength. Overall, the initial growth of $\Sigma(t)$ is followed by a small fluctuation around the saturation value, regardless of the strength of the quench. However, the way of $\Sigma(t)$ growth depends strongly on the quench strength. For $\delta\kappa$ below the critical value, $\Sigma(t)$ increases with larger oscillations and takes a long time to reach its saturation value with small oscillations. On the other hand, even though the growth of $\Sigma(t)$ still shows many oscillations for $\delta\kappa > \delta\kappa_c$ case, it saturates to a larger saturation value at a short time scale. At the critical quench $\delta\kappa = \delta\kappa_c$, $\Sigma(t)$ undergoes a fast growth which then quickly saturates to its saturation value with tiny fluctuations. We further note that the saturation values of $\Sigma(t)$ for $\delta\kappa \geqslant \delta\kappa_c$ are almost independent of the quench strength.

The rapid increase in $\Sigma(t)$ at the critical quench can be explained as follows. The ESQPT associated with the saddle point in the underlying classical system, which leads to the instability in the quantum many-body dynamics. Consequently,

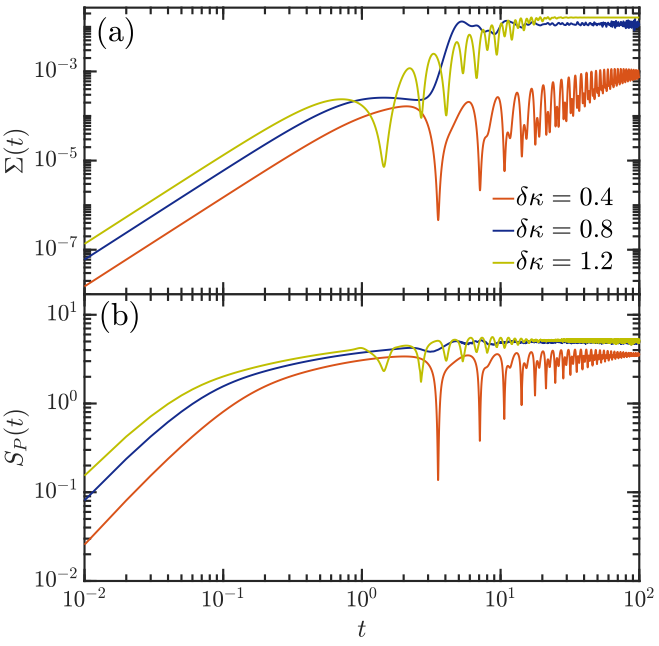

FIG. 4. (a) $\Sigma(t)$ as a function of t for several quench strengths $\delta\kappa$. (b) Time evolution of the energy distribution entropy $S_P(t)$ for different values of $\delta\kappa$. Other parameters: $N = 1000$, $\kappa_i = 0.4$, and $\delta\kappa_c = 0.8$ [see Eq. (8)].

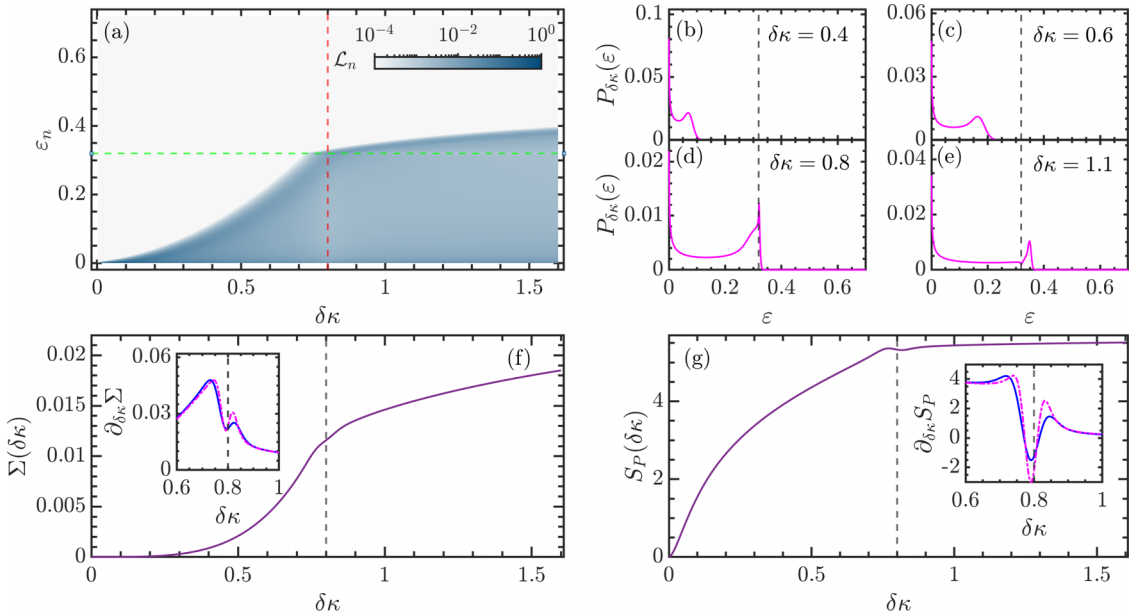

FIG. 5. (a) Heat map of the long-time-averaged Loschmidt echo spectrum $\mathcal{L}_n$ as a function of $\delta\kappa$ and ε_n with system size $N = 1000$. The horizontal dashed line marks the critical energy ε_c of the ESQPT, while the vertical red dashed line is the critical quench strength from Eq. (8). (b)–(e) Energy distribution of the long-time-averaged state $P_{\delta\kappa}(\varepsilon)$ for different values of $\delta\kappa$ with $N = 1000$. The vertical dashed line in each panel denotes the critical energy ε_c of the ESQPT, see Eq. (5). (f) Variance of the energy distribution of the long-time-averaged state as a function of $\delta\kappa$ for $N = 1000$. The inset shows $\partial_{\delta\kappa}\Sigma$ as a function of $\delta\kappa$ for $N = 1000$ (blue solid curve) and $N = 2000$ (magenta dot-dashed curve). (g) Entropy of the energy distribution of the long-time-averaged state as a function of $\delta\kappa$ for $N = 1000$. The inset plots $\partial_{\delta\kappa}S_P$ as a function of $\delta\kappa$ for $N = 1000$ (blue solid curve) and $N = 2000$ (magenta dot-dashed curve). The vertical dashed line in panels (f) and (g) is the critical quench strength $\delta\kappa_c$. Other parameters: $\kappa_i = 0.4$ and $\delta\kappa_c = 0.8$ obtained from Eq. (8).

the evolved state $\rho(t)$ is very spread out in the spectrum of the initial Hamiltonian in an extremely short time, as observed in Figs. 3(b) and 3(e). This results in the rapid growth in the variance of the energy distribution.

The observed features of $\Sigma(t)$ suggest that the underlying ESQPT leaves an imprint in the dynamics of quenched system. Hence, the evolution of $\Sigma(t)$ can be employed to distinguish different phases of an ESQPT. Moreover, the existence of the ESQPT can be efficiently signified by the rapid growth behavior in $\Sigma(t)$.

Figures 3(d) to 3(f) further demonstrate that the complexity of the evolved $P_t(\varepsilon)$ also shows a strong dependence on the quench strength. To measure the complexity of $P_t(\varepsilon)$, we study the entropy of $P_t(\varepsilon)$:

$$S_P(t) = -\int d\varepsilon P_t(\varepsilon) \ln P_t(\varepsilon). \tag{12}$$

It varies in the interval $S_P(t) \in [0, \ln \Delta\varepsilon]$ with $\Delta\varepsilon$ is the width of the energy spectrum. When the energy distribution is determined, that is, $P_t(\varepsilon) = 1$, we have $S_P(t) = 0$, while $S_P(t) = \ln \Delta\varepsilon$ implies $P_t(\varepsilon)$ is uniform, namely $P_t(\varepsilon) = (\Delta\varepsilon)^{-1}$.

Figure 4(b) shows the time evolution of $S_p(t)$ for the quench strengths that are the same as in Fig. 4(a). We see that the evolution of $S_P(t)$ is very similar to the behavior of $\Sigma(t)$, apart from small fluctuations around the saturation value. We also note that $S_P(t)$ saturates at a very short timescale in comparison with $\Sigma(t)$. However, due to the logarithmic definition in $S_P(t)$, the growth of $S_P(t)$ at the critical quench strength is not as rapid as in the case of $\Sigma(t)$. Nevertheless, the similarity between $S_P(t)$ and $\Sigma(t)$ means that both of them can be used to identify the occurrence and different phases of the ESQPT.

B. Long-time-averaged Loschmidt echo spectrum

The signatures of the ESQPT are also reflected in the long-time-averaged Loschmidt echo spectrum, which is calculated as

$$\begin{aligned}\mathcal{L}_n &= \lim_{T\to\infty} \frac{1}{T}\int_0^T L_n(t)dt \\ &= \lim_{T\to\infty} \frac{1}{T}\int_0^T dt \sum_{\alpha,\beta} \langle\psi_n|\alpha\rangle\langle\alpha|\psi_0\rangle\langle\beta|\psi_n\rangle\langle\psi_0|\beta\rangle \\ &\quad \times e^{-it(E_\alpha - E_\beta)} \\ &= \sum_\alpha |\langle\psi_n|\alpha\rangle|^2 |\langle\alpha|\psi_0\rangle|^2,\end{aligned} \tag{13}$$

where $H_f|\alpha\rangle = E_\alpha|\alpha\rangle$, $H_f|\beta\rangle = E_\beta|\beta\rangle$, and we carried out the integration as the energy spectrum of H_f is nondegenerate. The $\mathcal{L}_n$ can be recognized as the overlap between the long-time-averaged state $\bar{\rho} = \lim_{T\to\infty}\int_0^T \rho(t)dt$ and the nth eigenstate $\rho_n = |\psi_n\rangle\langle\psi_n|$ of H_i, so that $\mathcal{L}_n = \mathrm{Tr}(\bar{\rho}\rho_n)$. Here, we should point out that the final simplified form in the above equation only holds for the finite system. In the thermodynamic limit $N \to \infty$, as energy levels are degenerated at the ESQPT critical energy, the last equation in (13) is invalid. It is also worth mentioning that the reciprocal $\mathcal{L}_0$ is the participation ratio of the initial state $|\psi_0\rangle$ with respect to the eigenstates of H_f.

In Fig. 5(a), we plot the long-time-averaged Loschmidt echo spectrum $\mathcal{L}_n$ as a function of $\delta\kappa$ and ε_n for $\kappa_i = 0.4$ and $N = 1000$. We see that the ESQPT at $\delta\kappa_c = 0.8$ leads to a remarkable change in the behavior of $\mathcal{L}_n$, which, in turn, can be used to diagnose the onset of the ESQPT. Moreover, $\mathcal{L}_n$ for $\delta\kappa > \delta\kappa_c$ also shows a dip at the ESQPT critical energy ε_c, as marked by the horizontal dashed line in the figure. The dip observed in $\mathcal{L}_n$ at the critical energy for $\delta\kappa > \delta\kappa_c$ case is a consequence of the localization of the critical eigenstate $|\psi_c\rangle$ over the spectrum of H_f, which results in the significant contribution to $\mathcal{L}_n$ are the states with small values of $|\langle\psi_c|\alpha\rangle|^2$.

More information about the effect of the ESQPT are provided by the energy distribution of the long-time-averaged state weighted by $\mathcal{L}_n$,

$$P_{\delta\kappa}(\varepsilon) = \sum_n \mathcal{L}_n \delta(\varepsilon - \varepsilon_n). \tag{14}$$

Figures 5(b) to 5(e) demonstrate the energy distribution $P_{\delta\kappa}(\varepsilon)$ for several $\delta\kappa$ values. One can clearly see that $P_{\delta\kappa}(\varepsilon)$ exhibits distinct behaviors in different phases of the ESQPT. In particular, due to the localization of the critical eigenstate $|\psi_c\rangle$, the critical value of $\mathcal{L}_n$ is dominated by the large $|\langle\psi_c|\alpha\rangle|^2$ terms, when taking the system to the ESQPT critical energy. This means that, for the critical quench strength, the energy distribution has a sharp peak at the ESQPT critical energy, as observed in Fig. 5(d). This peak signals the ESQPT singularity and can be employed to probe the occurrence of the ESQPT.

To quantitatively investigate the features of $P_{\delta\kappa}(\varepsilon)$, as we did for the time-evolved energy distribution $P_t(\varepsilon)$, we study its variance and entropy, which are, respectively, defined by

$$\begin{aligned}\Sigma(\delta\kappa) &= \int d\varepsilon P_{\delta\kappa}(\varepsilon)[\varepsilon - \langle\varepsilon\rangle]^2,\\ S_P(\delta\kappa) &= -\int d\varepsilon P_{\delta\kappa}(\varepsilon)\ln P_{\delta\kappa}(\varepsilon),\end{aligned} \tag{15}$$

where $\langle\varepsilon\rangle = \int d\varepsilon P_{\delta\kappa}(\varepsilon)\varepsilon$.

In Fig. 5(f) we display $\Sigma(\delta\kappa)$ as a function of $\delta\kappa$ for $\kappa_i = 0.4$ and $N = 1000$. The variance $\Sigma(\delta\kappa)$ increases with increasing $\delta\kappa$, but it grows in different rate between two phases of the ESQPT. The changing of the growth rate in $\Sigma(\delta\kappa)$ occurs at the ESQPT critical quench strength due to the localized eigenstates around the ESQPT critical energy, which lead to the energy distribution remains almost unchanged for the quenches around $\delta\kappa_c$. This is confirmed by the derivative of the variance with respect to $\delta\kappa$, denoted by $\partial_{\delta\kappa}\Sigma(\delta\kappa)$, which is plotted in the inset of Fig. 5(f) for the cases of different system sizes. As we can see, $\partial_{\delta\kappa}\Sigma(\delta\kappa)$ shows an abrupt decrease and reaches its local minimal value near the critical quench strength. Hence, the variance $\Sigma(\delta\kappa)$ succinctly captures the signatures of the ESQPT.

The dependence of entropy $S_P(\delta\kappa)$ on the quench strength is plotted in Fig. 5(g). For $\delta\kappa < \delta\kappa_c$, $S_P(\delta\kappa)$ grows as $\delta\kappa$ increases, while it saturates to a stationary value as $\delta\kappa$ increases for $\delta\kappa > \delta\kappa_c$. This difference in the behavior of $S_P(\delta\kappa)$ allows us to use it to identify different phases of the ESQPT. In the neighborhood of the critical quench strength $\delta\kappa_c$, we see a decrease in $S_P(\delta\kappa)$. This means that the entropy $S_P(\delta\kappa)$ can be used as a witness of the ESQPT.

The eigenstates localization associated with the ESQPT critical point is also the source of the decrease of the entropy $S_P(\delta\kappa)$ near $\delta\kappa_c$. The localized eigenstates around the ESQPT critical energy give rise to small values of $P_{\delta\kappa}(\varepsilon)$ for the critical quench, as seen in Fig. 5(d). Hence, the entropy $S_P(\delta\kappa)$ would have a local minimal value at $\delta\kappa_c$. This is more visible in the inset of Fig. 5(f), where we show how the derivative of entropy $\partial_{\delta\kappa}S_P$ evolves as a function of $\delta\kappa$ for different system sizes. An obvious dip in the value of $\partial_{\delta\kappa}S_P$ appears near the critical quench strength, confirming that the entropy $S_P(\delta\kappa)$ undergoes a decrease as the strength of quench passes through its critical value. Increasing the system size N tends to sharpen the dip and moving its location to the critical value of $\delta\kappa$.

It is also interesting to investigate whether the Loschmidt echo spectrum can provide insights into the dynamics of $f_0 = \langle\hat{N}_0\rangle/N$, which has been used to study both ground-state QPT [68,71] and dynamical phase transition [20] in spin-1 BEC. The time-evolving f_0 is given by

$$\begin{aligned}\langle f_0(t)\rangle &= \frac{1}{N}\langle\psi_0|e^{iH_f t}\hat{N}_0 e^{-iH_f t}|\psi_0\rangle\\ &= \frac{1}{N}\sum_{n,m}\mathcal{A}_n^*(t)\mathcal{A}_m(t)N_{0,nm}\\ &= \frac{1}{N}\left[\sum_n L_n(t)N_{0,nn} + 2\sum_{n<m}\mathfrak{R}_{nm}\right],\end{aligned} \tag{16}$$

where $N_{0,k\ell} = \langle\psi_k|\hat{N}_0|\psi_\ell\rangle$, $\mathcal{A}_k(t) = \langle\psi_k|e^{-iH_f t}|\psi_0\rangle$ is the amplitude of $L_k(t)$, and

$$\mathfrak{R}_{nm} = \mathrm{Re}[\mathcal{A}_n^*(t)\mathcal{A}_m(t)N_{0,nm}], \tag{17}$$

denotes the real part of $\mathcal{A}_n^*(t)\mathcal{A}_m(t)N_{0,nm}$. Figure 6 plots $\mathfrak{R}_{nm}$ for different quenches at different times. We see that, regardless of the quench strength and time, the diagonal terms are much larger compared to the off-diagonal terms. This implies that the summation in Eq. (16) is governed by the diagonal terms, which are directly connected to the Loschmidt echo spectrum. The Loschmidt echo spectrum can therefore help us to understand the features that are exhibited in f_0 dynamics.

As a final remark of this section, we would like to point out that the Loschmidt echo spectrum can be experimentally detected by recent proposed protocols [89–91]. Moreover, we checked that the dynamical signatures of the ESQPT revealed in time-evolved and long-time-averaged Loschmidt echo spectrum can be observed in a several hundred milliseconds for the typical spin-spin interaction strength $|c|/h = 2\pi \times 9$ Hz [61]. These facts indicate that the experimental verification of our findings in the spin-1 BEC platform is achievable.

IV. CONCLUSION

In summary, by investigating the dynamical signatures of the ESQPT in the spin-1 BEC via the Loschmidt echo spectrum, we showed the usefulness of the Loschmidt echo spectrum in the studying of ESQPTs in quantum many-body systems. We explored how the ESQPT gets reflected in the behaviors of the Loschmidt echo spectrum and associated energy distribution.

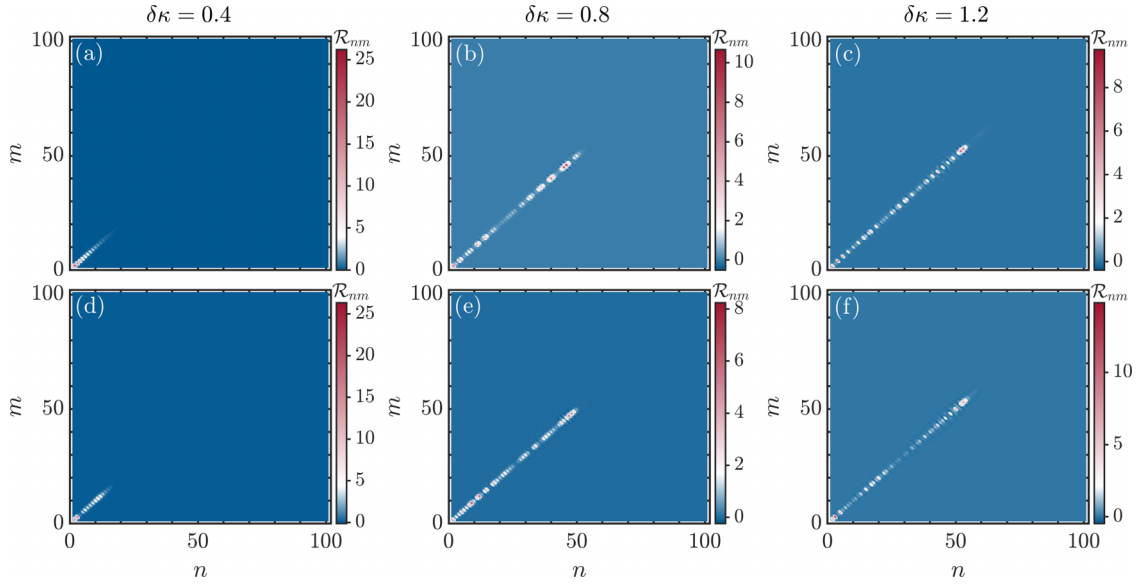

FIG. 6. $\mathfrak{R}_{nm}$ in Eq. (17) with respect to the nth and mth eigenstates of the initial Hamiltonian for three typical quenches at two times: (a)–(c) $t = 10$ and (d)–(f) $t = 100$. Other parameters: $N = 200$, $\kappa_i = 0.4$, and $\delta\kappa_c = 0.8$ obtained from Eq. (8).

The ESQPT in the spin-1 BEC is characterized by the logarithmic divergence of the density of states, which results in the localization of the eigenstates around the ESQPT. A detailed study of the classical limit of the system reveals that the presence of the ESQPT and the corresponding characterizations are a consequence of the saddle point in the classical system.

The analysis of the time evolution of the Loschmidt echo spectrum unveils that the underlying ESQPT leads to a drastic change in the behavior of the Loschmidt echo spectrum. In particular, we have seen that the singular behavior in the evolution of the Loschmidt echo spectrum signals the onset of the ESQPT. We further showed that the occurrence and different phases of the ESQPT were clearly identified in the properties of the energy distribution of the evolved state weighted by the components of the Loschmidt echo spectrum. In addition, an explicit examination of the long-time-averaged Loschmidt echo and associated energy distribution demonstrates that they can also be utilized to probe the ESQPT.

Although our conclusions are verified for spin-1 BEC, we would expect that qualitatively similar results should also be found in other systems that exhibit the logarithmic divergence in their density of states. A natural extension of the present work is to study the classification of the ESQPTs by performing scaling analyses on the critical behaviors of the Loschmidt echo spectrum. Classifying the ESQPTs is nontrivial and remains an open question. It would be also interesting to explore the relationship between the Loschmidt echo spectrum and the ESQPTs, which are signified by the discontinuity in the derivative of the density of states [3–5]. Finally, our findings extend the usefulness of the Loschmidt echo spectrum in studying of the dynamical quantum phase transitions [79] to ESQPTs, and open a different way to obtain a better understanding on the dynamical features of ESQPTs.

ACKNOWLEDGMENTS

This work is supported by the Zhejiang Provincial Nature Science Foundation (Grants No. LY20A050001 and No. LQ22A040006); the National Science Foundation of China under Grant No. 11805165; and the Slovenian Research Agency (ARRS) under Grant No. J1-4387.

[1] P. Cejnar, M. Macek, S. Heinze, J. Jolie, and J. Dobeš, J. Phys. A: Math. Gen. **39**, L515 (2006).
[2] M. Caprio, P. Cejnar, and F. Iachello, Ann. Phys. (NY) **323**, 1106 (2008).
[3] P. Stránský, M. Macek, and P. Cejnar, Ann. Phys. (NY) **345**, 73 (2014).
[4] P. Stránský and P. Cejnar, Phys. Lett. A **380**, 2637 (2016).
[5] P. Cejnar, P. Stránský, M. Macek, and M. Kloc, J. Phys. A: Math. Theor. **54**, 133001 (2021).
[6] A. L. Corps and A. Relaño, Phys. Rev. Lett. **127**, 130602 (2021).
[7] S. Sachdev, *Quantum Phase Transitions*, 2nd ed. (Cambridge University Press, Cambridge, England, 2011).
[8] F. Pérez-Bernal and F. Iachello, Phys. Rev. A **77**, 032115 (2008).
[9] M. Macek, P. Stránský, A. Leviatan, and P. Cejnar, Phys. Rev. C **99**, 064323 (2019).
[10] W.-T. Dong, Y. Zhang, B.-C. He, F. Pan, Y.-A. Luo, J. P. Draayer, and S. Karampagia, J. Phys. G: Nucl. Part. Phys. **48**, 045103 (2021).
[11] D. Larese, F. Pérez-Bernal, and F. Iachello, J. Mol. Struct. **1051**, 310 (2013).
[12] J. Khalouf-Rivera, F. Pérez-Bernal, and M. Carvajal, J. Quant. Spectrosc. Radiat. Transfer **261**, 107436 (2021).
[13] J. Khalouf-Rivera, M. Carvajal, and F. Pérez-Bernal, SciPost Phys. **12**, 002 (2022).

[14] V. M. Bastidas, P. Pérez-Fernández, M. Vogl, and T. Brandes, Phys. Rev. Lett. **112**, 140408 (2014).
[15] I. García-Mata, E. Vergini, and D. A. Wisniacki, Phys. Rev. E **104**, L062202 (2021).
[16] Q. Wang and F. Pérez-Bernal, Phys. Rev. E **104**, 034119 (2021).
[17] D. Mondal, S. Sinha, and S. Sinha, Phys. Rev. E **105**, 014130 (2022).
[18] Q.-W. Wang and S. Wu, Phys. Rev. A **102**, 063531 (2020).
[19] J. Chávez-Carlos, T. L. M. Lezama, R. G. Cortiñas, J. Venkatraman, M. H. Devoret, V. S. Batista, F. Pérez-Bernal, and L. F. Santos, arXiv:2210.07255.
[20] T. Tian, H.-X. Yang, L.-Y. Qiu, H.-Y. Liang, Y.-B. Yang, Y. Xu, and L.-M. Duan, Phys. Rev. Lett. **124**, 043001 (2020).
[21] P. Feldmann, C. Klempt, A. Smerzi, L. Santos, and M. Gessner, Phys. Rev. Lett. **126**, 230602 (2021).
[22] J. Cabedo and A. Celi, Phys. Rev. Res. **3**, 043215 (2021).
[23] B. Meyer-Hoppe, F. Anders, P. Feldmann, L. Santos, and C. Klempt, arXiv:2301.10655.
[24] L. Zhou, J. Kong, Z. Lan, and W. Zhang, arXiv:2209.11415.
[25] F. Leyvraz and W. D. Heiss, Phys. Rev. Lett. **95**, 050402 (2005).
[26] M. Šindelka, L. F. Santos, and N. Moiseyev, Phys. Rev. A **95**, 010103(R) (2017).
[27] D. J. Nader, C. A. González-Rodríguez, and S. Lerma-Hernández, Phys. Rev. E **104**, 064116 (2021).
[28] J. Gamito, J. Khalouf-Rivera, J. M. Arias, P. Pérez-Fernández, and F. Pérez-Bernal, Phys. Rev. E **106**, 044125 (2022).
[29] L. F. Santos and F. Pérez-Bernal, Phys. Rev. A **92**, 050101(R) (2015).
[30] L. F. Santos, M. Távora, and F. Pérez-Bernal, Phys. Rev. A **94**, 012113 (2016).
[31] P. Pérez-Fernández, P. Cejnar, J. M. Arias, J. Dukelsky, J. E. García-Ramos, and A. Relaño, Phys. Rev. A **83**, 033802 (2011).
[32] T. Brandes, Phys. Rev. E **88**, 032133 (2013).
[33] R. Puebla, A. Relaño, and J. Retamosa, Phys. Rev. A **87**, 023819 (2013).
[34] M. A. Bastarrachea-Magnani, S. Lerma-Hernández, and J. G. Hirsch, Phys. Rev. A **89**, 032101 (2014).
[35] R. Puebla, M.-J. Hwang, and M. B. Plenio, Phys. Rev. A **94**, 023835 (2016).
[36] A. Relaño, C. Esebbag, and J. Dukelsky, Phys. Rev. E **94**, 052110 (2016).
[37] P. Stránský, P. Cejnar, and R. Filip, Phys. Rev. A **104**, 053722 (2021).
[38] A. L. Corps and A. Relaño, Phys. Rev. A **105**, 052204 (2022).
[39] Q. Wang and F. Pérez-Bernal, Phys. Rev. E **103**, 032109 (2021).
[40] R. Puebla and A. Relaño, Phys. Rev. E **92**, 012101 (2015).
[41] Q. Wang and F. Pérez-Bernal, Phys. Rev. A **100**, 022118 (2019).
[42] Q. Wang and F. Pérez-Bernal, Phys. Rev. A **100**, 062113 (2019).
[43] A. Relaño, J. M. Arias, J. Dukelsky, J. E. García-Ramos, and P. Pérez-Fernández, Phys. Rev. A **78**, 060102(R) (2008).
[44] P. Pérez-Fernández, A. Relaño, J. M. Arias, J. Dukelsky, and J. E. García-Ramos, Phys. Rev. A **80**, 032111 (2009).
[45] M. Kloc, D. Šimsa, F. Hanák, P. R. Kaprálová-Žďánská, P. Stránský, and P. Cejnar, Phys. Rev. A **103**, 032213 (2021).
[46] M. Kloc, P. Stránský, and P. Cejnar, Phys. Rev. A **98**, 013836 (2018).
[47] Q. Hummel, B. Geiger, J. D. Urbina, and K. Richter, Phys. Rev. Lett. **123**, 160401 (2019).
[48] S. Pilatowsky-Cameo, J. Chávez-Carlos, M. A. Bastarrachea-Magnani, P. Stránský, S. Lerma-Hernández, L. F. Santos, and J. G. Hirsch, Phys. Rev. E **101**, 010202(R) (2020).
[49] P. Pérez-Fernández, A. Relaño, J. M. Arias, P. Cejnar, J. Dukelsky, and J. E. García-Ramos, Phys. Rev. E **83**, 046208 (2011).
[50] C. M. Lóbez and A. Relaño, Phys. Rev. E **94**, 012140 (2016).
[51] Á. L. Corps, R. A. Molina, and A. Relaño, J. Phys. A: Math. Theor. **55**, 084001 (2022).
[52] Á. L. Corps and A. Relaño, arXiv:2205.03443
[53] A. L. Corps and A. Relaño, Phys. Rev. B **106**, 024311 (2022).
[54] Á. L. Corps, P. Stránský, and P. Cejnar, arXiv:2212.08028.
[55] P. Pérez-Fernández and A. Relaño, Phys. Rev. E **96**, 012121 (2017).
[56] S. P. Kelly, E. Timmermans, and S.-W. Tsai, Phys. Rev. A **102**, 052210 (2020).
[57] M. R. Lambert, S.-W. Tsai, and S. P. Kelly, Phys. Rev. A **106**, 012206 (2022).
[58] R. Puebla and A. Relaño, Europhys. Lett. **104**, 50007 (2014).
[59] B. Dietz, F. Iachello, M. Miski-Oglu, N. Pietralla, A. Richter, L. von Smekal, and J. Wambach, Phys. Rev. B **88**, 104101 (2013).
[60] Y. Kawaguchi and M. Ueda, Phys. Rep. **520**, 253 (2012).
[61] D. M. Stamper-Kurn and M. Ueda, Rev. Mod. Phys. **85**, 1191 (2013).
[62] J. Stenger, S. Inouye, D. M. Stamper-Kurn, H.-J. Miesner, A. P. Chikkatur, and W. Ketterle, Nature (London) **396**, 345 (1998).
[63] L. E. Sadler, J. M. Higbie, S. R. Leslie, M. Vengalattore, and D. M. Stamper-Kurn, Nature (London) **443**, 312 (2006).
[64] F. Gerbier, A. Widera, S. Fölling, O. Mandel, and I. Bloch, Phys. Rev. A **73**, 041602(R) (2006).
[65] C. D. Hamley, C. S. Gerving, T. M. Hoang, E. M. Bookjans, and M. S. Chapman, Nat. Phys. **8**, 305 (2012).
[66] L. Zhao, J. Jiang, T. Tang, M. Webb, and Y. Liu, Phys. Rev. A **89**, 023608 (2014).
[67] X.-Y. Luo, Y.-Q. Zou, L.-N. Wu, Q. Liu, M.-F. Han, M. K. Tey, and L. You, Science **355**, 620 (2017).
[68] C. B. Dağ, S.-T. Wang, and L.-M. Duan, Phys. Rev. A **97**, 023603 (2018).
[69] W. Zhang, S. Yi, and L. You, New J. Phys. **5**, 77 (2003).
[70] Z. Zhang and L.-M. Duan, Phys. Rev. Lett. **111**, 180401 (2013).
[71] M. Xue, S. Yin, and L. You, Phys. Rev. A **98**, 013619 (2018).
[72] D. Jacob, L. Shao, V. Corre, T. Zibold, L. De Sarlo, E. Mimoun, J. Dalibard, and F. Gerbier, Phys. Rev. A **86**, 061601(R) (2012).
[73] M. Anquez, B. A. Robbins, H. M. Bharath, M. Boguslawski, T. M. Hoang, and M. S. Chapman, Phys. Rev. Lett. **116**, 155301 (2016).
[74] Y. Liu, S. Jung, S. E. Maxwell, L. D. Turner, E. Tiesinga, and P. D. Lett, Phys. Rev. Lett. **102**, 125301 (2009).
[75] E. M. Bookjans, A. Vinit, and C. Raman, Phys. Rev. Lett. **107**, 195306 (2011).
[76] J. Jiang, L. Zhao, M. Webb, and Y. Liu, Phys. Rev. A **90**, 023610 (2014).
[77] A. Vinit and C. Raman, Phys. Rev. A **95**, 011603(R) (2017).
[78] H.-Y. Liang, L.-Y. Qiu, Y.-B. Yang, H.-X. Yang, T. Tian, Y. Xu, and L.-M. Duan, New J. Phys. **23**, 033038 (2021).
[79] C. Y. Wong and W. C. Yu, Phys. Rev. B **105**, 174307 (2022).
[80] M. Rautenberg and M. Gärttner, Phys. Rev. A **101**, 053604 (2020).

[81] W. Zhang, D. L. Zhou, M.-S. Chang, M. S. Chapman, and L. You, Phys. Rev. A **72**, 013602 (2005).
[82] M. C. Gutzwiller, *Chaos in Classical and Quantum Mechanics*, Vol. 1 (Springer Science & Business Media, New York, 2013).
[83] K. Husimi, Proc. Phys. Math. Soc. Jpn **22**, 264 (1940).
[84] Q. Wang and H. T. Quan, Phys. Rev. E **96**, 032142 (2017).
[85] S. Pappalardi, A. Russomanno, B. Žunkovič, F. Iemini, A. Silva, and R. Fazio, Phys. Rev. B **98**, 134303 (2018).
[86] T. Xu, T. Scaffidi, and X. Cao, Phys. Rev. Lett. **124**, 140602 (2020).
[87] K. Hashimoto, K.-B. Huh, K.-Y. Kim, and R. Watanabe, J. High Energy Phys. 11 (2020) 068.
[88] R. A. Kidd, A. Safavi-Naini, and J. F. Corney, Phys. Rev. A **103**, 033304 (2021).
[89] B. Swingle, G. Bentsen, M. Schleier-Smith, and P. Hayden, Phys. Rev. A **94**, 040302(R) (2016).
[90] D. V. Vasilyev, A. Grankin, M. A. Baranov, L. M. Sieberer, and P. Zoller, PRX Quantum **1**, 020302 (2020).
[91] C. B. Dag, S. I. Mistakidis, A. Chan, and H. R. Sadeghpour, arXiv:2210.03840.